Mo P60

Hidden Information in Ill-posed Inverse Problems

S.S. Kahrobaei* (Delft University of Technology), M. Mansoori (Delft University of Technology), G.J.P. Joosten (Shell Global Solutions International B.V.), P.M.J. Van den Hof (Eindhoven University of Technology) & J.D. Jansen (Delft University of Technology)

SUMMARY

It is well known that parameter updating of large-scale numerical reservoir flow models (a.k.a. 'computer assisted history matching') is an ill-posed inverse problem. Typically the number of uncertain parameters in a reservoir flow model is very large whereas the available information for estimating these parameters is limited. The classic solution to this problem is to regularize the unknowns, e.g. by penalizing deviations from a prior model. Attempts to estimate all uncertain parameters from production data without regularization typically lead to unrealistically high parameter values and therefore to updated parameter fields that have little or no geological realism. However, it has been suggested that the application of unregularized reservoir parameter estimation may still add value, because it, sometimes, gives an indication of the location of significant missing features in the model. We investigated under which conditions this perceived added value might occur. We conducted several twin experiments and applied unregularized parameter estimation to update uncertain parameters in a simple two-dimensional reservoir model that contained a major deficiency in the form of a missing high or low permeability feature. We found that in case of low-permeability barriers or high-permeability streaks it is indeed sometimes possible to localize the position of the model deficiency. To further analyze this behavior we conducted one-dimensional experiments using a transfer function formalism to characterize the identifiability of the location and magnitude of model deficiencies (flow barriers).

Introduction

Bayesian parameter estimation

Estimating reservoir parameters from measured data is usually an ill-posed inverse problem due to the large number of parameters and the limited amount of data (Shah et al., 1978; Oliver et al., 2008). The ill-posed nature of the problem leads to unreliable results. A classic way to restore well-posedness is regularization through introducing additional information. This can be done by, e.g., specifying a strong spatial correlation, zonation, expansion in terms of a limited number of basis functions, penalizing deviations from a prior model, or a combination of these methods. Penalizing deviations from a prior model forms a natural consequence of applying a Bayesian approach to updating an uncertain prior, using uncertain data, to obtain a less uncertain posterior (Tarantola, 2005; Oliver et al., 2008). The penalty term makes the problem well-posed, restricts the parameter updates to values that keep the posterior values not too far from the prior values, and generally increases the smoothness of the results. On the other hand, attempts to estimate all uncertain parameters from production data without regularization typically lead to very high or low parameter values that have little or no geological realism. It is also well known that the estimated parameter values in such unregularized ill-posed problems are extremely sensitive to noise in the data.

Model maturation

Joosten et al. (2011) introduced the *model maturation* concept and showed that sometimes the application of unregularized reservoir parameter estimation still appears to have added value. They showed that localized unrealistic parameter values can be used as an indicator of model errors (or *under-modeling*) in the underlying reservoir model. The objective of the present paper is to investigate some of the theoretical aspects of model maturation, i.e. to determine why and under which conditions there is relevant information hidden in the results of unregularized ill-posed inverse problems.

Approach

In our approach to investigate the model maturation concept we first use 'twin experiments' in which computer-assisted history matching of one or more priors (i.e. reservoir models) is performed using synthetic data, generated with the aid of a 'synthetic truth' (i.e. another reservoir model). The synthetic truth has a significant flow-relevant feature (e.g. a flow barrier or a high permeability streak) which is missing in the prior models. In the second part of the paper we analyze the identifiability of a flow barrier for a one-dimensional (1D) case in the frequency domain.

Objective function

In a Bayesian framework, reservoir history matching can be formulated as a minimization problem. The underlying assumption is usually that the prior model can be characterized by mean values and a covariance matrix of the uncertain parameters (Oliver et al., 2008). The objective function then consist of a quadratic mismatch term and a term that penalizes deviations of the parameters from their prior mean values:

$$J(\boldsymbol{\theta}) = \underbrace{\left(\mathbf{d}-\mathbf{h}(\boldsymbol{\theta})\right)^T \mathbf{P}_d^{-1}\left(\mathbf{d}-\mathbf{h}(\boldsymbol{\theta})\right)}_{\text{data mismatch term}} + \underbrace{\left(\boldsymbol{\theta}-\bar{\boldsymbol{\theta}}\right)^T \mathbf{P}_\theta^{-1}\left(\boldsymbol{\theta}-\bar{\boldsymbol{\theta}}\right)}_{\text{regularization term}}, \tag{1}$$

where $\boldsymbol{\theta}$ is a vector of unknown model parameters and $\bar{\boldsymbol{\theta}}$ a vector of their mean values, $\mathbf{d}$ is a vector of data (measurements), $\mathbf{h}$ is a vector valued-function that relates the model parameters to the model outputs (i.e. the simulated data), and $\mathbf{P}_d$ and $\mathbf{P}_\theta$ are covariance matrices of data errors and model parameters respectively. The unregularized objective function does not contain the regularization term:

$$J(\boldsymbol{\theta}) = \left(\mathbf{d}-\mathbf{h}(\boldsymbol{\theta})\right)^T \mathbf{P}_d^{-1}\left(\mathbf{d}-\mathbf{h}(\boldsymbol{\theta})\right). \tag{2}$$

Minimization of the objective function is achieved by adjustment of the model parameters $\boldsymbol{\theta}$, usually subject to constraints on their values. Various numerical techniques are available to perform this minimization, the most efficient one being gradient-based minimization where the gradient is computed using the adjoint method (Oliver et al., 2008). For the present study we used an in-house reservoir simulator with adjoint-functionality and an iterative gradient-based minimization procedure.

Experimental results

Reservoir model

As a first step we use a simple 2D reservoir model with a five-spot water injection-production configuration to investigate the model maturation approach. The reservoir is horizontal and divided in $21 \times 21 = 441$ grid blocks of size 33.33m × 33.33m × 2m. The constant porosity is 0.3, the initial water saturation is 0.2, and the initial reservoir pressure is 30 MPa. The four producers, located at the corners are operated at a constant bottom hole pressure of 25 MPa, without rate constraints, and the water injector at the center at a constant water flow rate of 0.002 m^3/s, without pressure constraints. Oil and water viscosities are $\mu_o = 5 \times 10^{-3}$ Pa s, $\mu_w = 1 \times 10^{-3}$ Pa s, oil, rock and water compressibilities are $c_o = 1.0 \times 10^{-9}$ Pa^{-1}, $c_r = 1.0 \times 10^{-10}$ Pa^{-1}, and $c_w = 1.0 \times 10^{-10}$ Pa^{-1}, and relative permeabilities are described with Corey exponents $n_o = n_w = 2$, connate water saturation $S_{wc} = 0.2$, residual oil saturation $S_{or} = 0.2$, and end-point relative permeabilities $k^0_{ro} = 0.9$ and $k^0_{rw} = 0.6$. Production is simulated for 1500 days, corresponding to 1.47 moveable pore volumes injected. Wells are located in the grid block centers, and we use a standard Peaceman well inflow model with a well bore radius $r_w = 0.10$ m.

Permeability field

The uncertainty in the permeability field is expressed by an ensemble of 500 model realizations. The ensemble members are generated by unconditioned sequential Gaussian simulation from a lognormal distribution with mean of 300 mD and a standard deviation of 100 mD, and a spherical variogram with a nugget of 0.001 and a range of 1000 meters. One of the ensemble members is chosen as the 'synthetic truth' after adding a flow-relevant feature, i.e. a barrier or a high perm streak. The mean and covariance of the prior are calculated based on the remaining 499 realizations. Figure 1 shows the 'true' permeability field before addition of a flow-relevant feature, the mean value of the prior and the covariance matrix of the prior. The maximum permeability of the true field is 492 mD, the minimum 205 mD, and the average 387 mD.

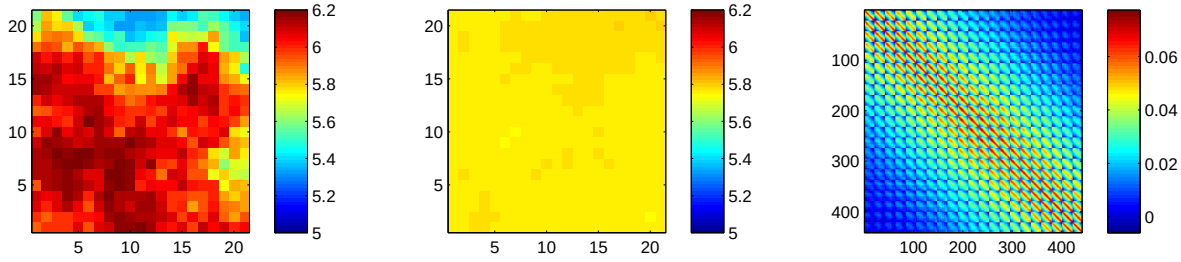

Figure 1 *From left to right: true permeability field, mean value of the prior, and covariance matrix of the prior. All permeability values are expressed as the natural logarithm of permeability in mD.*

The synthetic truth is used to generate synthetic historical data in the form of measured oil and water rates in the producers. Independent measurement errors are generated from Gaussian distributions with zero mean and a standard deviation equal to 10% percent of the original measurements. Negative production rates, after the addition of noise, are reset to zero. Because the measurements errors are independent, the error covariance matrix is diagonal. The permeabilities of those grid blocks that contain wells are not updated in the minimization process to avoid localization of the updates in just the well grid blocks. We performed different sets of 'twin experiments', using four 'truth cases', each

containing different flow-relevant features, and the two objective functions represented in equation (1) and equation (2).

Experiment # 1: Truth case with a sealing fault – regularized objective function.

In this experiment the truth contains a sealing fault, which separates production well *prod2* in the bottom-right corner from the rest of the field. The presence of this fault results in a lower oil production and later water breakthrough in well *prod2* compared to the other wells. Figure 2 depicts the true permeability field with the well locations. The black line represents the sealing fault, which is modelled by means of a dimensionless seal factor $0 \leq \sigma \leq 1$ modifying the inter-grid block transmissibilities T according to

$$T_{eff} = \sigma T \,. \tag{3}$$

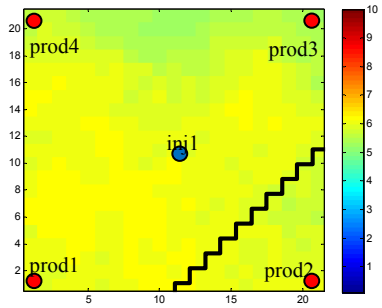

Figure 2 *Truth case with well locations. The black line represents a sealing fault.*

The fault in the truth model is not present in the prior model. We use the regularized objective function, given by equation (1), and minimize it by adjustment of the permeability in each grid block. After 137 iterations the objective function mismatch is reduced to about one third of its original value and, because no further reduction occurs, the minimization process is stopped. Figure 3 depicts the prior and updated permeability fields.

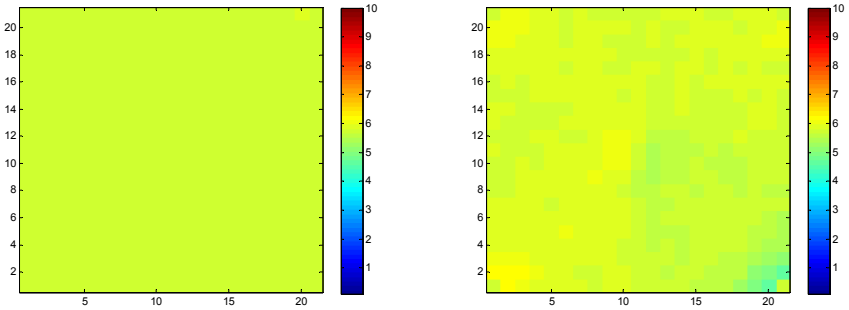

Figure 3 *Prior permeability field (left), and updated permeability field (right) for experiment #1.*

The updated permeability field stays close to the prior and does not show any unphysical updates. Some small adjustment of the permeability close to well *prod2* is visible, but any sign of the sealing fault is absent. Figure 4 depicts the oil and water rates in the four producers for the truth, the prior, and the updated model. As can be seen in Figure 4, the simulated data for the updated model poorly match the historical data, especially for well *prod2*.

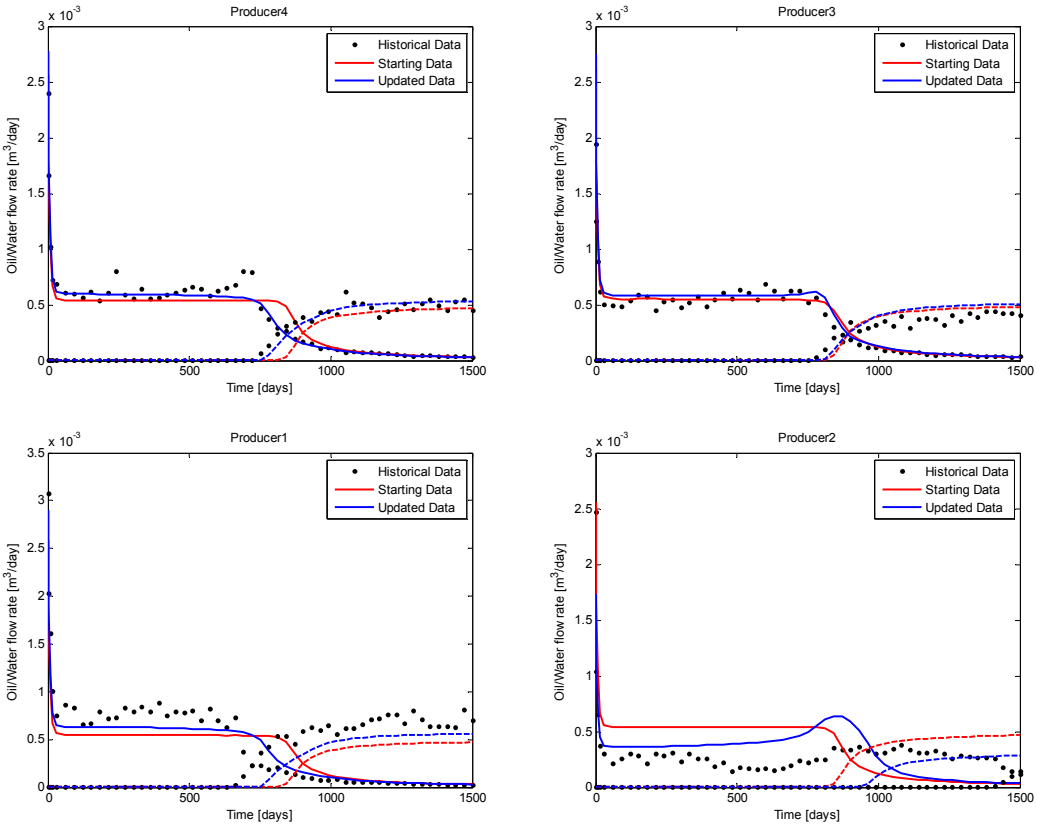

Figure 4 *Data match in the producers for experiment #1. Black dots indicate the measured oil and water rates. Solid and dashed red lines are the oil and water rates of the prior model. Solid and dashed blue lines are the oil and water rates of the updated model.*

Experiment # 2 - Truth case with a sealing fault – unregularized objective function.

In this experiment we use the same truth as in experiment #1 (see Figure 2), but we use the unregularized objective function given by equation (2). Different permeability fields, randomly chosen from the ensemble of 499 members, were used as starting values for the iterative minimization procedure. In addition, the mean of the ensemble was also chosen as one of the starting models. The minimizations converged in about 500 to 600 iterations, in which the objective function mismatch reduced with three orders of magnitude. Figure 5 shows four different starting models and their updates after history matching. In all four cases a low permeable band, with permeabilities between 1 to 10 mD is visible in the updated permeability fields. This low permeable band is apparently generated in order to match the production for well *prod2*, which is separated from the other wells through the sealing fault in the truth case. The low-permeable band, which has very low permeability values compared to other part of the fields, is apparently indicating that something is missing in our starting models. I.e., in this example, the unrealistic updates resulting from history matching with an unregularized objective function indeed seem to give an indication for under-modeling. Figure 6 depicts the oil and water rates in the four producers for the truth, the prior, and the updated model. As can be seen in Figure 6, the simulated data for the updated model match the historical data near-perfectly. In all the experiments from now on we will only use the unregularized objective function given by equation (2).

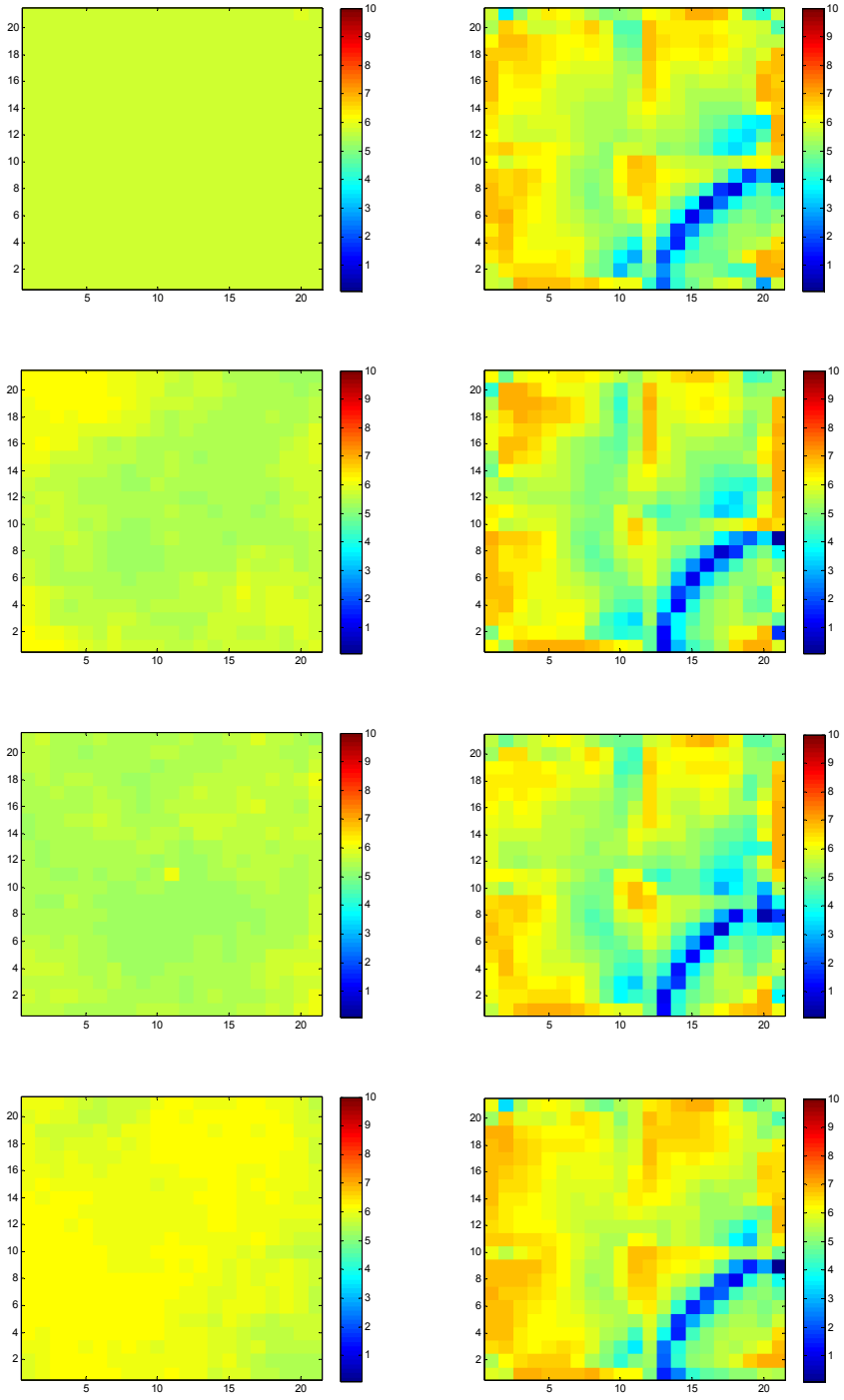

Figure 5 *Different models used as starting values for the minimization procedure (left), and the updated models (right) for experiment #2. The starting model in the top row is the ensemble average.*

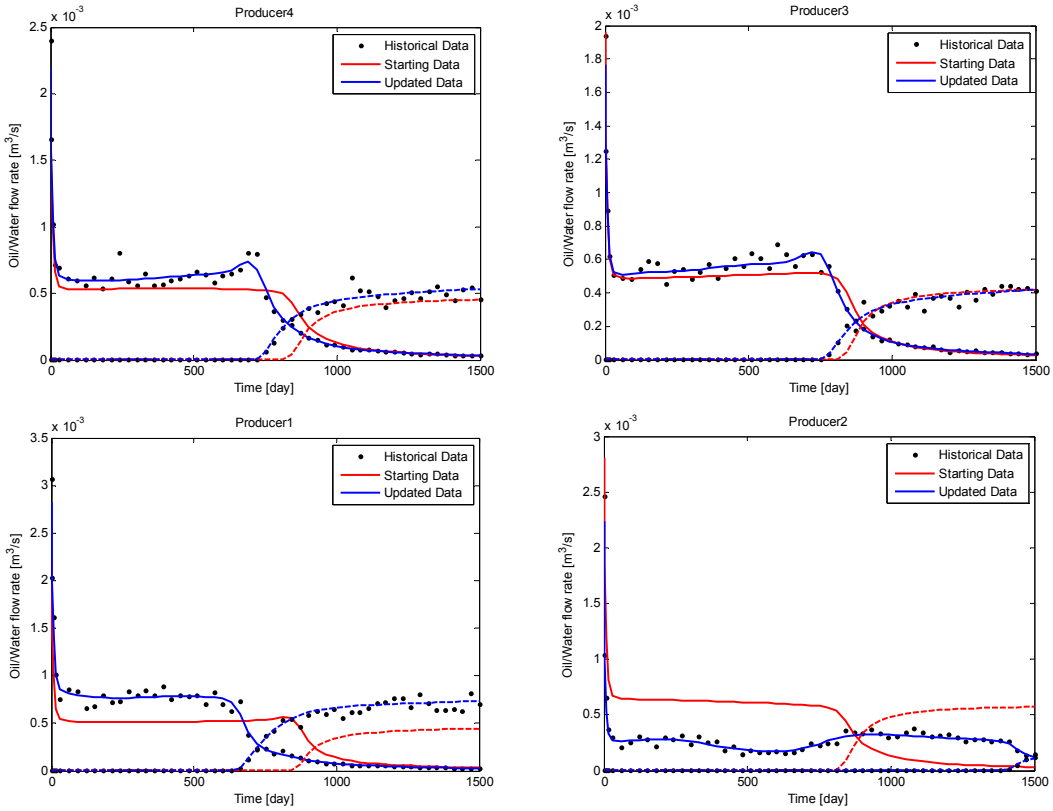

Figure 6 *Data match in the producers for experiment #2. Black dots indicate the measured oil and water rates. Solid and dashed red lines are the oil and water rates of the prior model. Solid and dashed blue lines are the oil and water rates of the updated model.*

Experiment # 3 - Capturing the position of a sealing fault.

In this experiment the sealing fault in the truth case has a different location than in the previous experiments and is located closer to the well *prod2*. Figure 7 depicts the true permeability field together with the location of the sealing fault.

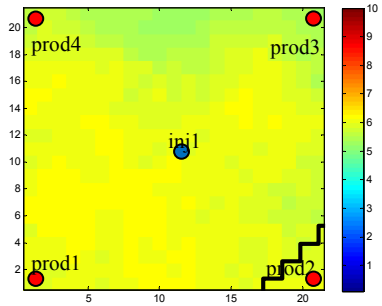

Figure 7 *Truth for experiment #3.*

Just like in experiment #2, the updated permeability field is obtained by minimization of the unregularized objective function given by equation (2). Figure 8 shows the starting model and its update after history matching. It can be seen that the low permeable band is now generated closer to well *prod2*, as is the location of the fault in the synthetic truth. In terms of data mismatch, we again obtained a near-perfect match between the updated model and the truth, while also the flow rates in the wells were again matched near-perfectly. This example indicates that apparently the production information in the wells also carries some information about the location of the fault.

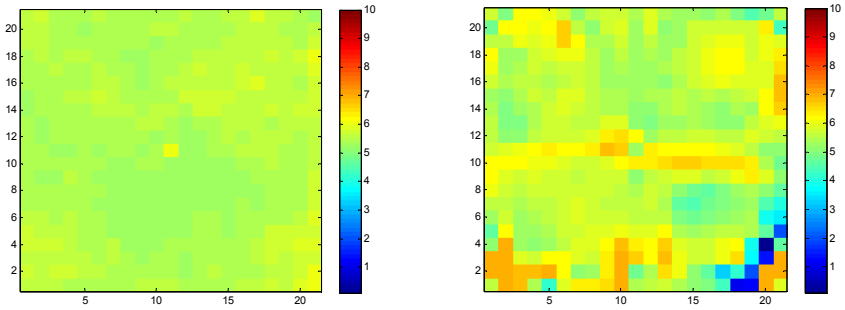

Figure 8 *Starting model (left) and updated model (right) for experiment #3.*

Experiment # 4 - Capturing the shape of a sealing fault

In this experiment the shape of the sealing fault is changed from a diagonal stair-step line to a large hook in the vicinity of well *prod2*. Figure 9 depicts the true permeability field, and Figure 10 the starting model and its update after history matching. As can be seen in Figure 10, the shape of the low permeable region is different compared to what we obtained in experiment #2. In this case we end up with a square-shaped low permeable region in the vicinity of well *prod2*. In terms of data mismatch, we got a good match between updated model and the truth model. This example indicates that apparently the production information in the wells also carries some information about the shape of the fault.

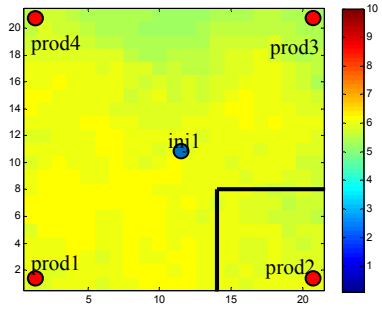

Figure 9 *Truth for experiment #4.*

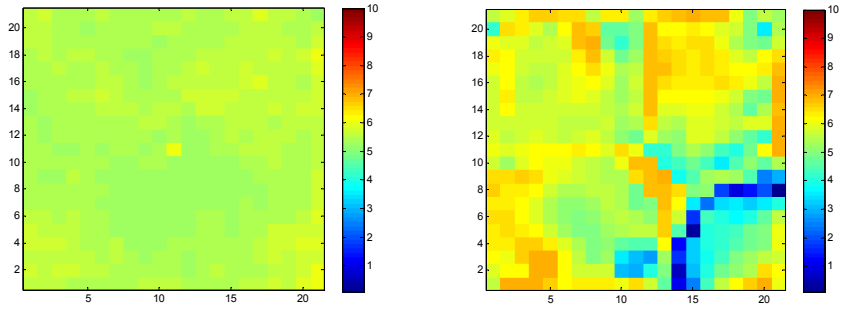

Figure 10 *Starting model (left) and updated model (right) for experiment #4.*

Experiment # 5 – Effect of measurement errors.

In this set of experiments we investigate the effect of measurement errors. The truth case is the same as in experiment #2, but the errors in the observed data are chosen differently. Figure 11 shows the updated permeability fields for measurements with measurement errors with standard deviations of 5%, 15%, 20% and 25% of the original measured values. It is clear from Figure 11 that increasing error levels lead to increasingly worse permeability estimates. For the 25% case the updated model contains completely spurious bands of low-permeability values.

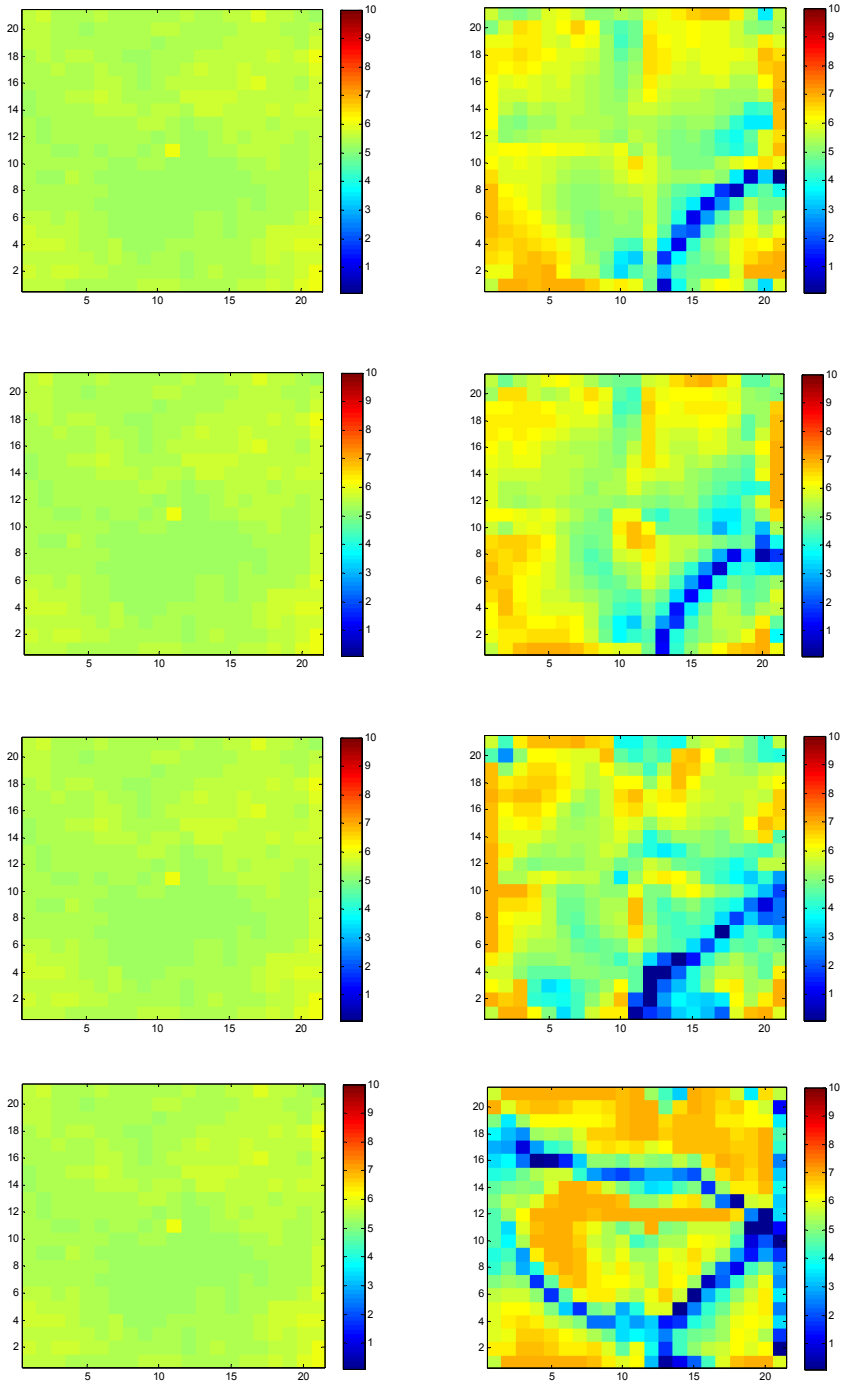

Figure 11 *Starting model (left) and its updates (right) for different measurement errors for experiment #5.From top to bottom: 5%, 15%, 20% and 25% error.*

Experiment # 6 - Truth case with a high perm channel

In this experiment instead of a sealing fault as a significant flow-relevant feature, we introduce a high-permeability channel in the truth. The high-perm channel is missing in the starting model used in the history matching procedure. The background permeability field is the same as in the previous experiments, but a channel with a permeability of 7000 mD connects producer *prod2* to injector *inj1*; see Figure 12. Figure 13 shows the starting model and its updates after 85 iterations. The permeability of the red band in the updated model in Figure 13 is 230000 to 4500000 mD. Figure 14 shows the data match for the four producers. Again this example confirms that history matching with an unregularized objective function may reveal some information about flow-relevant features.

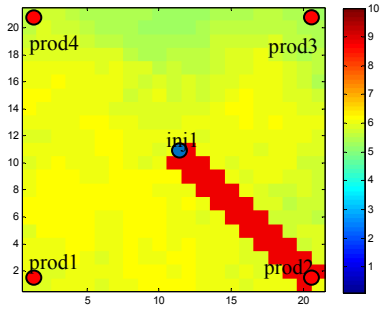

Figure 12 *Truth for experiment #6. The red grid blocks form a high-perm streak.*

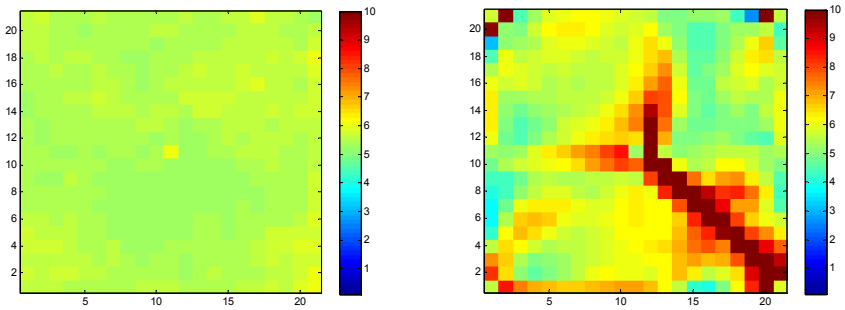

Figure 13 *Starting model (left) and its update (right) for experiment #6.*

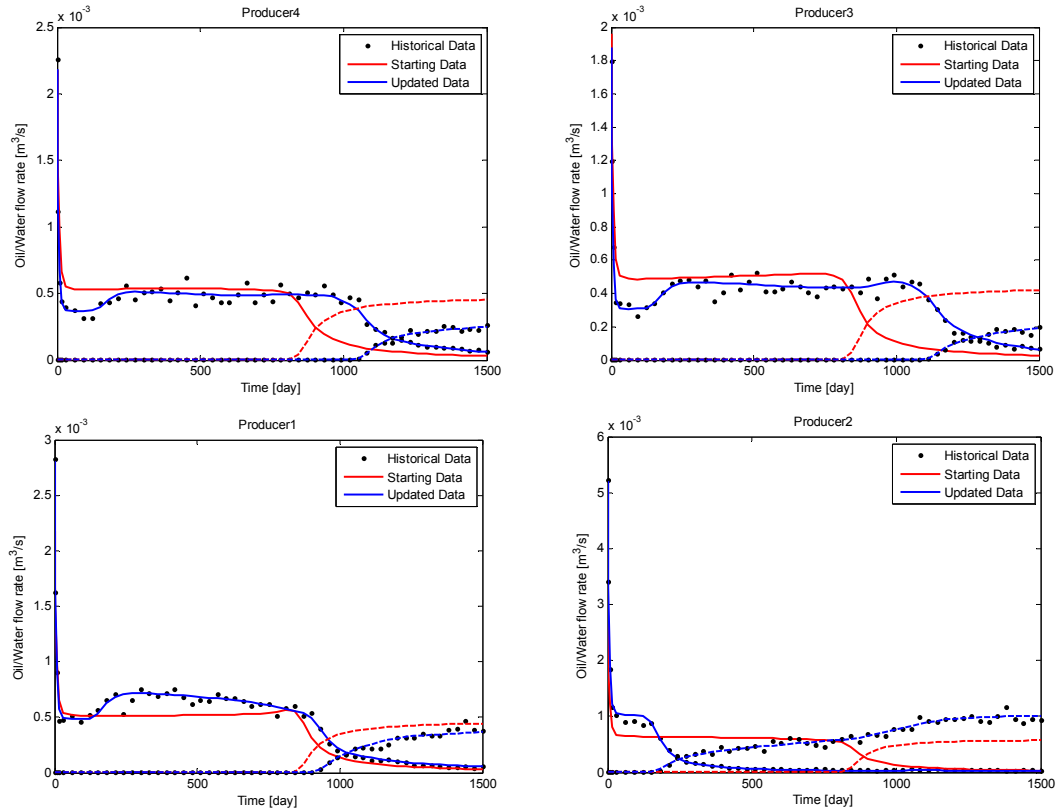

Figure 14 *Data match in the producers for experiment #6. Black dots indicate the measured oil and water rates. Solid and dashed red lines are the oil and water rates of the prior model. Solid and dashed blue lines are the oil and water rates of the updated model.*

Identifiability

The system-theoretical analysis of the presence of information in measured data is centered around the concept of identifiability. The parameters in a model are identifiable if they can be uniquely estimated from measured output data by a suitable choice of the control input.

Watson et al. (1984) and Datta Gupta et al. (1997) considered identifiability in steady-state (incompressible) two-phase flow and concluded that identifiability of reservoir properties is limited to average properties between wells. However, we consider (slightly) compressible flow and time-varying well rates, and it is well known from classical well testing (pressure transient analysis), and from related methods such as pulse testing or interference testing, that information about the distance between wells and flow-relevant features (e.g. reservoir boundaries or sealing faults) is sometimes present in the data, although to a limited extent due to the diffusive nature of pressure transients; see, e.g., Grader and Horne (1988) and Ahn and Horne (2010).

Zandvliet et al. (2008) and Van Doren (2010) addressed identifiability in reservoir systems from a system-theoretical point of view. They conclude that the number of identifiable parameters in a reservoir model based on input-output measurements in wells is very limited, and, moreover, can only be identified if the input is 'sufficiently exciting'. However, using a singular value decomposition (SVD) of the sensitivity matrix $d\mathbf{h}(\boldsymbol{\theta}) / d\boldsymbol{\theta}$, they also show that it is sometimes possible to identify large-scale flow-relevant features, as captured by the first SVD basis functions. Here, we will follow another approach, and use a transfer function formalism to characterize the identifiability of the location and magnitude of flow barriers in 1D experiments.

Transfer function formalism

Frequency response

In systems and control theory it is standard to analyze the dynamic behavior of a system by considering its response in the frequency domain. A sensitivity analysis of the frequency response shows how different parameters affect the system's dynamic behavior. The same approach can be followed to investigate the effect of the presence of a low permeable barrier in a reservoir. For the sake of simplicity, a 1D homogeneous injection-production system with a single fault (i.e. a low permeable barrier) is considered. It is assumed that this system contains a single-phase slightly compressible fluid, such that its behavior can be approximated as linear in the pressure. The 1D reservoir model can be considered as a system consisting of three blocks with lengths L_a, L_b and L_c; see Figure 15. The total length $L = L_a + L_c$ and the length L_b of the middle block are known, but the position of the middle block (given by L_a) is unknown.

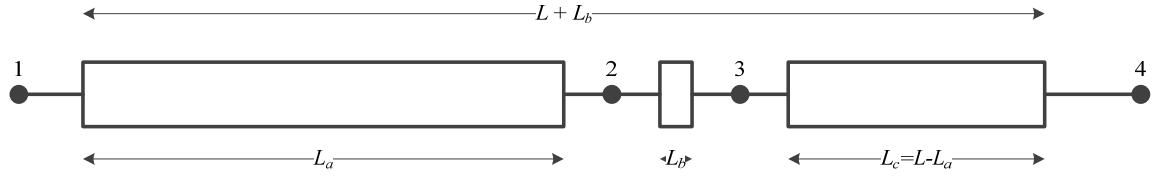

Figure 15 *Schematic representation of two 1D domains separated by a low permeable barrier.*

Input-output relations and transfer functions

The frequency response of a system containing multiple elements can conveniently be described with transfer functions, which describe the output from the system elements as a function of their input in the frequency domain or the Laplace domain. In order to find the input-output relations for porous-media flow we need to start from the pressure diffusion equation for 1D flow,

$$\frac{\partial p(x,t)}{\partial t} = \eta \frac{\partial^2 p(x,t)}{\partial x^2}, \tag{4}$$

where p is pressure, x is space, t is time, and η is the inverse of the hydraulic diffusivity D:

$$\eta = \frac{1}{D} = \frac{k}{\varphi \mu c_t}. \tag{5}$$

Here k is permeability, φ is porosity, μ is fluid viscosity and c_t is total compressibility. The flow rate q can be written as

$$q(x,t) = -A\frac{k}{\mu}\frac{\partial p(x,t)}{\partial x}, \tag{6}$$

where A is surface area, which is taken as one in our analysis. By applying a Laplace transform to equation (4) with zero initial condition we obtain,

$$\left(\frac{\partial^2}{\partial x^2} - \frac{s}{\eta}\right)\mathcal{P}(x,s) = 0, \tag{7}$$

which can be expressed as

$$\left(\frac{\partial}{\partial x} - \sqrt{\frac{s}{\eta}}\right)\left(\frac{\partial}{\partial x} + \sqrt{\frac{s}{\eta}}\right)\mathcal{P}(x,s) = 0, \tag{8}$$

and which has a solution of the form

$$\mathcal{P}(x,s) = C_1 e^{x\sqrt{\frac{s}{\eta}}} + C_2 e^{-x\sqrt{\frac{s}{\eta}}}. \tag{9}$$

In the same way the flow rate can be written in the Laplace domain as

$$\mathcal{Q}(x,s) = -\frac{k}{\mu}C_1\sqrt{\frac{s}{\eta}}e^{x\sqrt{\frac{s}{\eta}}} + \frac{k}{\mu}C_2\sqrt{\frac{s}{\eta}}e^{-x\sqrt{\frac{s}{\eta}}}. \tag{10}$$

The functions C_1 and C_2 can be determined by requiring the solution to satisfy given boundary conditions for $\mathcal{P}(x_{outlet},s)$ at the outlet and $\mathcal{Q}(x_{inlet},s)$ at the inlet, resulting in

$$\mathcal{P}(x_{inlet},s) = \frac{2}{e^{-x_{outlet}\sqrt{\frac{s}{\eta}}} + e^{x_{outlet}\sqrt{\frac{s}{\eta}}}}\mathcal{P}(x_{outlet},s) - \frac{\mu}{k}\sqrt{\frac{\eta}{s}}\frac{e^{-x_{outlet}\sqrt{\frac{s}{\eta}}} - e^{x_{outlet}\sqrt{\frac{s}{\eta}}}}{e^{-x_{outlet}\sqrt{\frac{s}{\eta}}} + e^{x_{outlet}\sqrt{\frac{s}{\eta}}}}\mathcal{Q}(x_{inlet},s), \tag{11}$$

$$\mathcal{Q}(x_{outlet},s) = \frac{k}{\mu}\sqrt{\frac{s}{\eta}}\frac{e^{-x_{outlet}\sqrt{\frac{s}{\eta}}} - e^{x_{outlet}\sqrt{\frac{s}{\eta}}}}{e^{-x_{outlet}\sqrt{\frac{s}{\eta}}} + e^{x_{outlet}\sqrt{\frac{s}{\eta}}}}\mathcal{P}(x_{outlet},s) + \frac{2}{e^{-x_{outlet}\sqrt{\frac{s}{\eta}}} + e^{x_{outlet}\sqrt{\frac{s}{\eta}}}}\mathcal{Q}(x_{inlet},s). \tag{12}$$

Subsequently $\mathcal{Q}(x_{outlet},s)$ and $\mathcal{P}(x_{inlet},s)$ can be written as a function of $\mathcal{P}(x_{outlet},s)$ and $\mathcal{Q}(x_{inlet},s)$ as

$$\begin{bmatrix}\mathcal{Q}(x_{outlet},s)\\ \mathcal{P}(x_{inlet},s)\end{bmatrix} = \begin{bmatrix}A_{11} & A_{12}\\ A_{21} & A_{22}\end{bmatrix}\begin{bmatrix}\mathcal{Q}(x_{inlet},s)\\ \mathcal{P}(x_{outlet},s)\end{bmatrix}, \tag{13}$$

where the matrix elements A_{ij}, which represent the various input-output relations, can be derived as

$$A_{11} = \frac{2}{e^{x_{outlet}\sqrt{\frac{s}{\eta}}} + e^{-x_{outlet}\sqrt{\frac{s}{\eta}}}}, \tag{14}$$

$$A_{12} = \frac{k}{\mu}\sqrt{\frac{s}{\eta}}\,\frac{e^{-x_{outlet}\sqrt{\frac{s}{\eta}}} - e^{x_{outlet}\sqrt{\frac{s}{\eta}}}}{e^{x_{outlet}\sqrt{\frac{s}{\eta}}} + e^{-x_{outlet}\sqrt{\frac{s}{\eta}}}}, \tag{15}$$

$$A_{21} = \frac{\mu}{k}\sqrt{\frac{\eta}{s}}\,\frac{e^{x_{outlet}\sqrt{\frac{s}{\eta}}} - e^{-x_{outlet}\sqrt{\frac{s}{\eta}}}}{e^{x_{outlet}\sqrt{\frac{s}{\eta}}} + e^{-x_{outlet}\sqrt{\frac{s}{\eta}}}}, \tag{16}$$

$$A_{22} = \frac{2}{e^{x_{outlet}\sqrt{\frac{s}{\eta}}} + e^{-x_{outlet}\sqrt{\frac{s}{\eta}}}}. \tag{17}$$

In this way we can derive the transfer functions for each block of our system. Finally, by coupling the transfer functions, we can derive the input-output relations for the entire system. Figure 16 shows the coupled model in block diagram representation for our 1D reservoir model, where we used the letters *A*, *B* and *C* to indicate the three consecutive blocks of Figure 15.

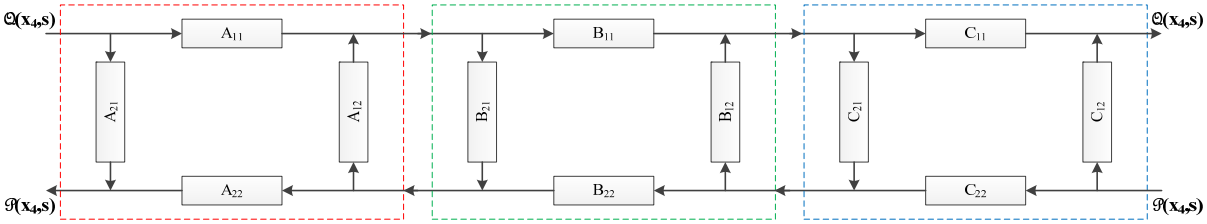

Figure 16 *Coupled model in block diagram representation.*

Each block of Figure 16 has an input-output relation in the form of equation (13). Consequently, by performing matrix multiplications, we can find the transfer functions that represent the input-output relations for the entire system. The matrix form of the input-output relations can be written as

$$\begin{bmatrix} \mathcal{Q}(x_{outlet},s) \\ \mathcal{P}(x_{inlet},s) \end{bmatrix} = \begin{bmatrix} S_{11} & S_{12} \\ S_{21} & S_{22} \end{bmatrix} \begin{bmatrix} \mathcal{Q}(x_{inlet},s) \\ \mathcal{P}(x_{outlet},s) \end{bmatrix}, \tag{18}$$

where the elements S_{ij} are given by

$$S_{11} = -\frac{A_{11}B_{11}C_{11}}{C_{21}\left(B_{12} + A_{12}B_{11}B_{22} - A_{12}B_{12}B_{21}\right) + A_{12}B_{21} - 1}, \tag{19}$$

$$\begin{aligned} S_{12} = -\frac{1}{A_{12}B_{21} + C_{21}B_{12} + A_{12}C_{21}B_{11}B_{22} - A_{12}C_{21}B_{12}B_{21} - 1} \times \\ \left[C_{12} - A_{12}C_{12}B_{21} + C_{11}C_{22}B_{12} - C_{12}C_{21}B_{12} + \right. \\ A_{12}C_{11}C_{22}B_{11}B_{22} - A_{12}C_{11}C_{22}B_{12}B_{21} - \\ \left. A_{12}C_{12}C_{21}B_{11}B_{22} + A_{12}C_{12}C_{21}B_{12}B_{21}\right] \end{aligned} \tag{20}$$

$$\begin{aligned} S_{21} = -\frac{1}{A_{12}F_{21} + C_{21}B_{12} + A_{12}C_{21}B_{11}B_{22} - A_{12}C_{21}B_{12}B_{21} - 1} \times \\ \left[A_{21} + A_{11}A_{22}B_{21} - A_{12}A_{21}B_{21} - A_{21}C_{21}B_{12} - \right. \\ A_{21}C_{21}B_{12} + A_{11}A_{22}C_{21}B_{11}B_{22} - A_{11}A_{22}C_{21}B_{12}B_{21} - \\ \left. A_{12}A_{21}C_{21}B_{11}B_{22} + A_{12}A_{21}C_{21}B_{12}B_{21}\right] \end{aligned} \tag{21}$$

$$S_{22} = -\frac{A_{22}C_{22}B_{22}}{A_{12}\left(B_{21} + C_{21}B_{11}B_{22} - C_{21}B_{12}B_{21}\right) + C_{21}B_{12} - 1}. \tag{22}$$

Effect of a low permeable barrier

In the 2D twin experiments we used flow rates in the injector and pressures in the producers as inputs, and flow rates in the producers as outputs. In the following we will therefore focus on the behavior of the transfer functions S_{11} (from flow at the inlet to flow at the outlet) and S_{12} (from pressure at the outlet to flow at the outlet). First we consider the sensitivity of S_{11} to changes in the magnitude of the barrier permeability k_b for a fixed barrier location $L_a = 150$ m. In that case the sensitivity matrix $d\mathbf{h}(\boldsymbol{\theta}) / d\boldsymbol{\theta}$ reduces to a scalar dS_{11} / dk_b, and Figure 17 depicts its magnitude as a function of frequency for different values of k_b. It can be seen that the sensitivity increases for decreasing barrier permeabilities, i.e. the barrier becomes more identifiable for decreasing permeabilities. This effect is also visible in Figure 18, which depicts the sensitivity dS_{12} / dk_b as a function of frequency. Next we consider the sensitivities of the output with respect to the location L_a of the barrier for a fixed permeability value of 0.1 mD. The corresponding values of dS_{11} / dL_a and dS_{12} / dL_a have been depicted in Figures 19 and 20. These results indicate that, for this example, identifiability of the barrier location increases with an increase in distance of the barrier from the producer for S_{11}, while the opposite occurs for S_{12}, i.e. an increase in identifiability with increasing distance from the injector. Further analysis will be required to generalize these results.

Table 1 *Parameter values.*

Parameter	*Magnitude*	*Units*
φ	0.2	-
μ	10^{-3}	Pa s
c_t	10^{-7}	1/Pa
A	1	m^2
L	500	m
L_b	10	m

Conclusions

We conducted several twin experiments and applied unregularized parameter estimation to update uncertain parameters in a simple 2D reservoir model that contained a major deficiency in the form of a missing high or low permeability feature. We found that, in case of low-permeability barriers or high-permeability streaks, it is sometimes possible to localize the position of the model deficiency, and, to a lesser extent, the permeability magnitude of these features.

To further analyze this behavior we conducted 1D experiments using a transfer function formalism (i.e. a dynamic response analysis in the frequency domain) to characterize the identifiability of the location and magnitude of a flow barrier. The results indicate that, for this example, identifiability of the permeability magnitude of the barrier increases with a decrease in permeability magnitude, while identifiability of the barrier location increases with an increase in distance of the barrier from either the injector or the producer, depending on the location of inputs and outputs.

Further analysis will be required to assess the differences in identifiability between barrier magnitude and barrier location, and, in particular, to assess to what extent the findings remain valid for larger and geologically more complex reservoirs.

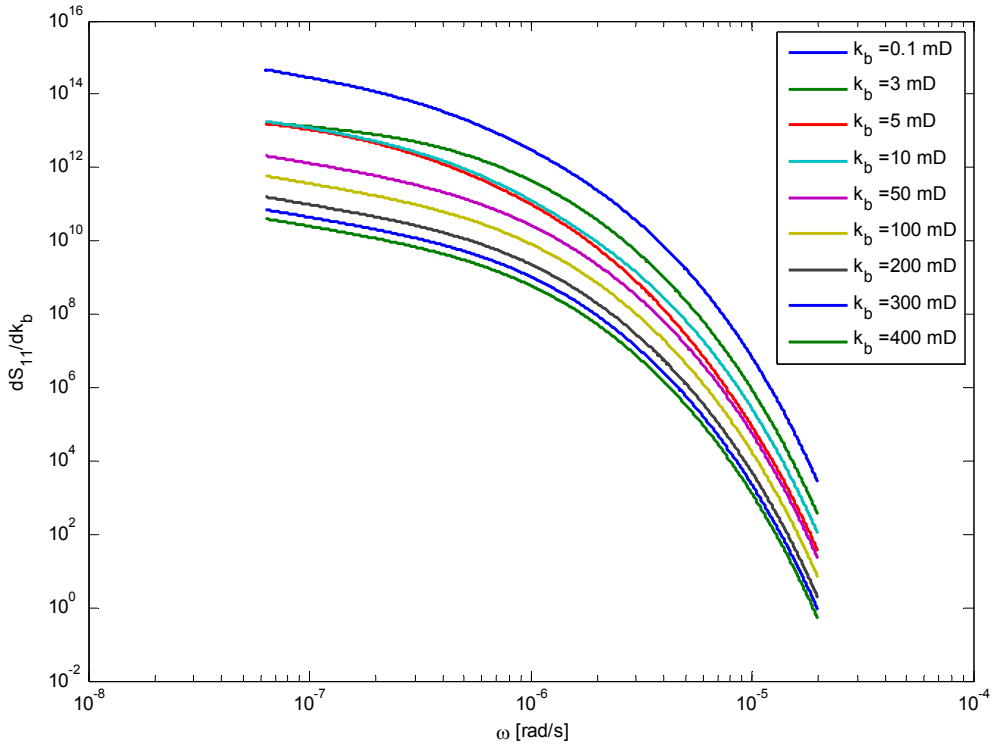

Figure 17 *Sensitivity of the frequency response S_{11} to the barrier permeability k_b as a function of frequency □ for different values of the barrier permeability.*

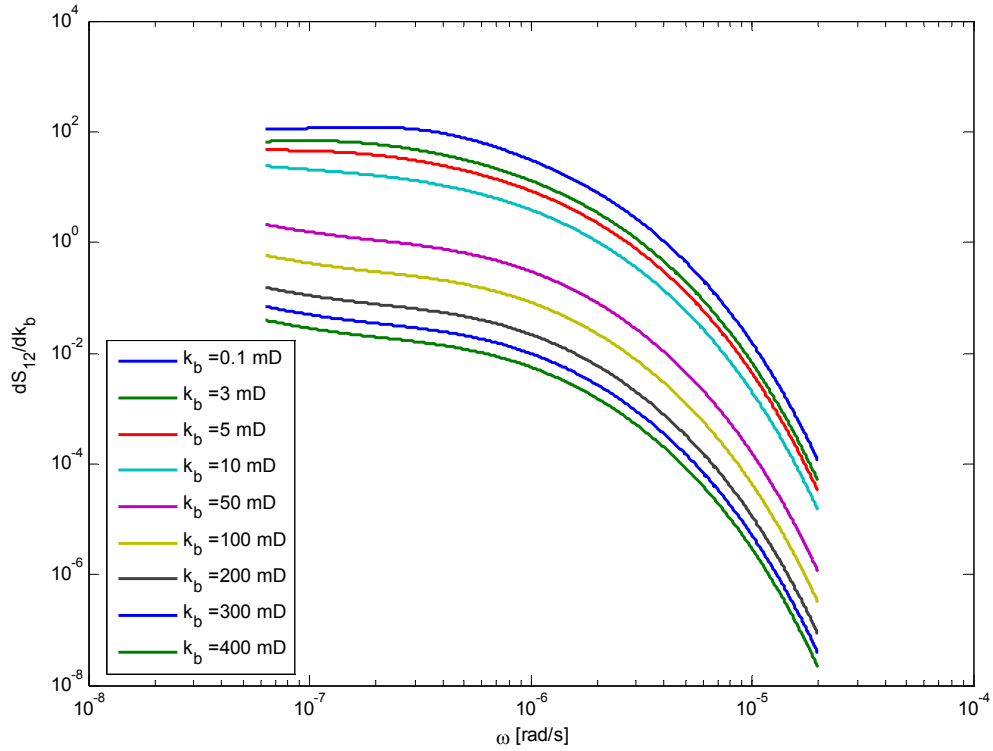

Figure 18 *Sensitivity of the frequency response S_{12} to the barrier permeability k_b as a function of frequency □ for different values of the barrier permeability.*

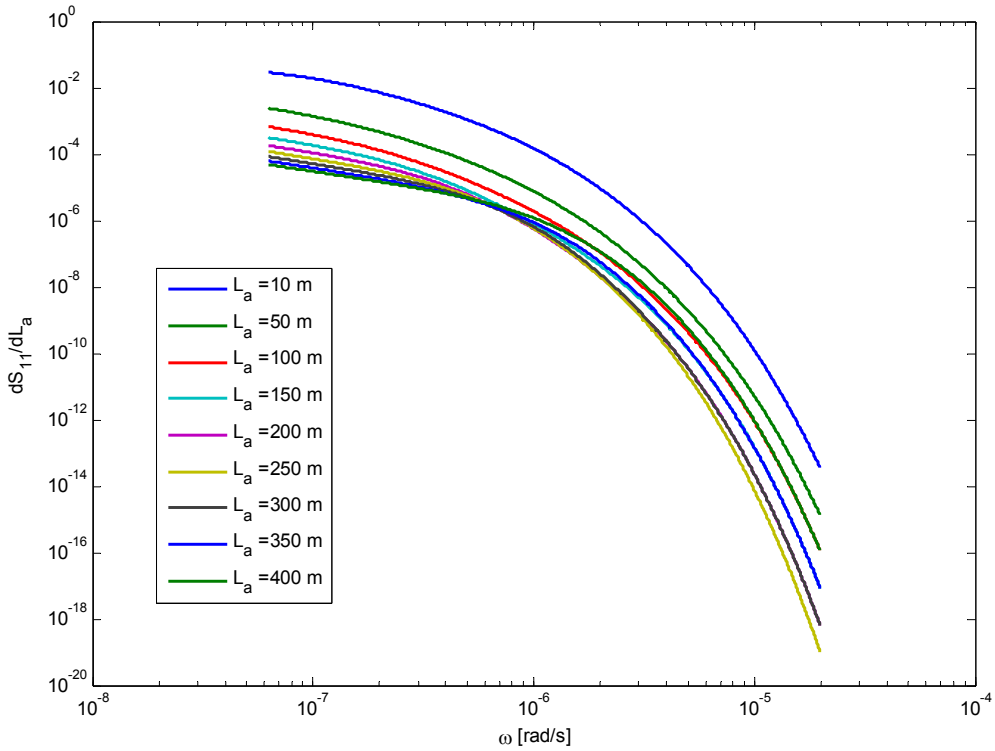

Figure 19 *Sensitivity of the frequency response S_{11} to the barrier location L_a as a function of frequency □ for different values of the barrier location.*

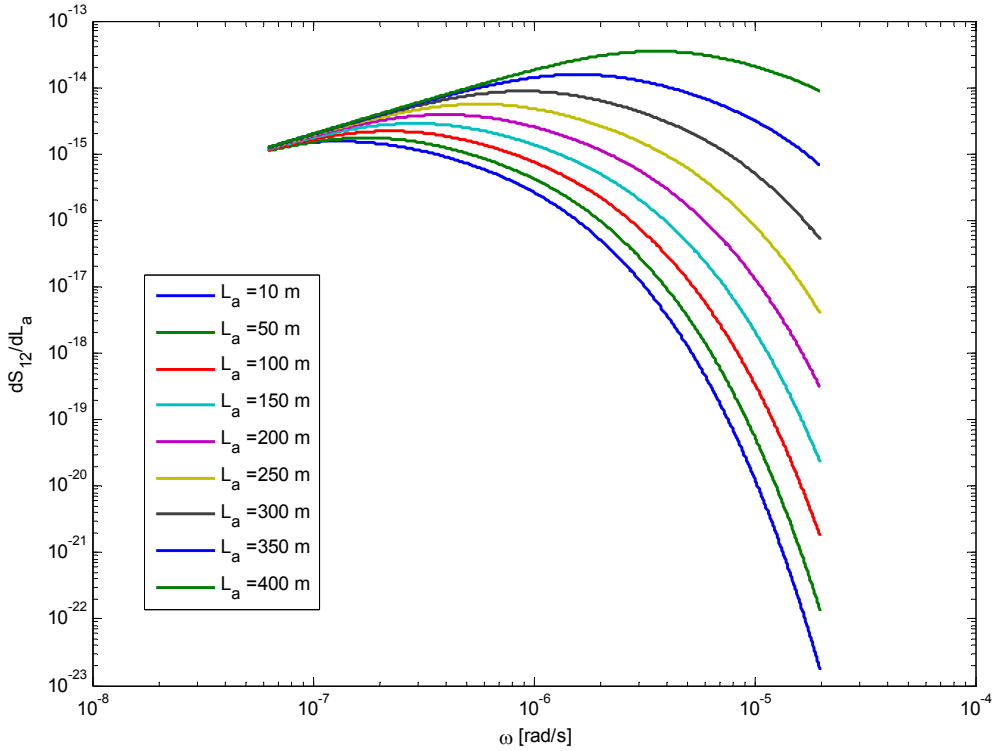

Figure 20 *Sensitivity of the frequency response S_{12} to the barrier location L_a as a function of frequency □ for different values of the barrier location.*

Acknowledgements

The authors acknowledge Shell Global Solutions International for sponsoring this research through the Recovery Factory program, and prof. Rashtchian of Sharif University of Technology, Iran, for supporting the assignment of Mehdi Mansoori to TU Delft and TU Eindhoven.

References

Ahn, S. and Horne R.N. [2010] Estimating Permeability Distributions From Pressure Pulse testing. *Paper SPE 134391 presented at the SPE Annual technical Conference and Exhibition*, Florence, Italy, 19-22 September.

Byrd, R.H., Lu, P., Nocedal, J. and Zhu, C. [1995] A limited memory algorithm for bound constrained optimization. *SIAM Journal on Scientific Computing*, **16**(5), 1190-1208.

Datta-Gupta, A., Vasco, D. W. and Long, J.C.S. [1997] On the sensitivity and spatial resolution of transient pressure and tracer data for heterogeneity characterization. *SPE Formation Evaluation*, **12**(2), 137-144.

Grader, A.S. and Horne, R.N. [1988] Interference Testing: Detecting a Circular Impermeable or Compressible Subregion. *SPE Formation Evaluation*, **3**(2), 420-428.

Joosten, G.J.P., Altintas, A. and Sousa, P.D. [2011] Practical and Operational Use of Assisted History Matching and Model-Based Optimisation in the Salym Field. *Paper SPE-146697-MS presented at the SPE Annual Technical Conference and Exhibition*, Denver, Colorado, USA, 30 October-2 November 2011.

Oliver, D.S., Reynolds, A.C. and Liu, N. [2008] *Inverse theory for petroleum reservoir characterization and history matching.* Cambridge University Press.

Shah, P.C., Gavalas, G.R. and Seinfeld, J.H. [1978] Error Analysis in History Matching: The Optimum Level of Parameterization. *Society of Petroleum Engineers Journal*, **18**(3), 219-228.

Stewart, G. [2011] *Well test analysis and design*. PennWell, Tulsa.

Tarantola, A. [2005] *Inverse problem theory and methods for model parameter estimation*. SIAM, Philadelphia.

Van Doren, J.F.M., Van den Hof, P.M.J., Jansen, J.D. and Bosgra, O.H. [2008] Determining identifiable parameterizations for large-scale physical models in reservoir engineering. In: M. Chung, P. Misra, H. Shim (eds.) *Proc. 17th International Federation for Automatic Control (IFAC) World Congress*, 11421-11426, Seoul, Korea, 6-11 July.

Van Doren, J.F.M. [2010] Model structure analysis for model-based operation of petroleum reservoirs. *PhD thesis, Delft University of Technology*.

Watson, A.T., Gavalas, G.R. and Seinfeld, J.H. [1984] Identifiability of Estimates of Two-Phase Reservoir Properties in History Matching. *SPE Journal*, **24**(6), 697-706.

Zandvliet, M.J., van Doren, J.F.M., Bosgra, O.H., Jansen, J.D. and van den Hof, P.M.J. [2008] Controllability, observability and identifiability in single-phase porous media flow. *Computational Geosciences*, **12**(4), 605-622.